


Defibrinogenation Ameliorates Retinal Microgliosis and Inflammation in A CX3CRI-Independent Manner

ASN Neuro
Volume 14: 1–18
© The Author(s) 2022
Article reuse guidelines:
sagepub.com/journals-permissions
DOI: 10.1177/17590914221131446
journals.sagepub.com/home/asn


Borna Sarker^{1,2}, Sandra M. Cardona^{1,2}, Kaira A. Church^{1,2},
Difernando Vanegas^{1,2}, Priscila Velazquez^{1,2}, Colin Rorex^{1,2},
Derek Rodriguez^{1,2}, Andrew S. Mendiola³, Timothy S. Kern^{4,5},
Nadia D. Domingo⁶, Robin Stephens^{6,7}, Isabel A. Muzzio⁸,
and Astrid E. Cardona^{1,2} 

Abstract

Microglia-mediated inflammation plays a significant role in neuronal and vascular damage in diabetic retinopathy (DR), but the mechanism linking inflammation, neurodegeneration, and impaired vascular integrity is still unclear. Previous studies from diabetic mouse models showed accumulation of fibrinogen at vessel lesions surrounded by perivascular microglial clusters. The purpose of this study was to evaluate whether the pathological hallmarks of gliosis and vascular aberrations characterized in diabetic animal models are consistent with those in diabetic human retinas, and to assess the effects of the defibrinogenating agent anicrod in retinal pathology and visual acuity in a two-hit inflammatory diabetic mouse model. Post-mortem human eyes were assessed for retinal and inflammatory gene expression by quantitative PCR. Immunohistochemical analyses in human and murine retinas were performed using markers of gliosis, vascular integrity, and fibrinogen deposition. An inflammatory microenvironment, with microgliosis and microaneurysms, was found in the diabetic human eye. Microglial activation, fibrinogen deposition, and axonal loss were also observed in the diabetic murine retina. Anicrod treatment correlated with reduced microgliosis, less fibrinogen deposition, and reduced pro-inflammatory cytokine levels in diseased retinal tissues. Together, these data suggest that fibrinogen contributes to microglia-mediated inflammation in the diabetic retina. Since retinal microgliosis, vascular pathology, and vision deficits manifest in diabetic mice irrespective of CX3CRI genotype, our results indicate that defibrinogenation can dampen systemic neuroinflammation and vascular insults, thereby improving vision at early stages of diabetes.

Summary Statement

Diabetic human and murine retinas revealed pronounced microglial morphological activation and vascular abnormalities associated with inflammation. Pharmacological fibrinogen depletion using anicrod dampened microglial morphology alterations, resolved fibrinogen accumulation, rescued axonal integrity, and reduced inflammation in the diabetic murine retina.

Keywords

microglia, diabetic retinopathy, fibrinogen, inflammation, anicrod, visual acuity

Received July 18, 2022; Revised September 14, 2022; Accepted for publication September 20, 2022

¹Department of Molecular Microbiology and Immunology, The University of Texas at San Antonio, San Antonio, TX, USA

²South Texas Center for Emerging Infectious Diseases, The University of Texas at San Antonio, San Antonio, TX, USA

³Gladstone Institute of Neurological Disease, San Francisco, CA, USA

⁴Department of Ophthalmology, Gavin Herbert Eye Institute, University of California-Irvine, Irvine, CA, USA

⁵Veterans Administration Medical Center Research Service, Long Beach, CA, USA

⁶Rutgers Center of Immunity and Inflammation, Rutgers New Jersey Medical School, Newark, NJ, USA

⁷Department of Pharmacology, Physiology and Neuroscience, Rutgers Center of Immunity and Inflammation, Rutgers New Jersey Medical School, Newark, NJ, USA

⁸Department of Psychological and Brain Sciences, The University of Iowa, Iowa City, IA, USA

Corresponding Author:

Astrid E. Cardona, Department of Molecular Microbiology and Immunology, South Texas Center for Emerging Infectious Diseases, The University of Texas at San Antonio, One UTSA Circle, San Antonio, TX 78249, USA.

Email: astrid.cardona@utsa.edu



Introduction

Diabetic retinopathy (DR) is a microvascular complication of diabetes mellitus, associated with vasculature permeability and leakage of blood proteins into the surrounding tissue. Chronic systemic inflammation from secondary infections is a common feature of diabetes, characterized by elevated serum levels of endotoxins, inflammatory mediators, and acute-phase proteins, such as C-reactive protein, plasminogen activator inhibitor-1, and fibrinogen (Festa et al., 2002; Kern, 2007; Spranger et al., 2003; Wellen & Hotamisligil, 2005). Increased concentrations of proinflammatory mediators and angiogenic factors in the vitreous of diabetic patients with retinopathy further support the involvement of inflammation in DR (Adamec-Mroczek et al., 2009; Boss et al., 2017; Bromberg-White et al., 2013; Burgos et al., 1997; Doganay et al., 2002; Funatsu et al., 2005; Jain et al., 2013; Klaassen et al., 2017; Loukovaara et al., 2014; Mao & Yan, 2014; Schoenberger et al., 2012; Vujosevic et al., 2016; Wang et al., 2009; Wu et al., 2017). However, the exact mechanisms by which acute-phase proteins and coagulation factors, including fibrinogen, contribute to inflammation and neurodegeneration in DR remain unclear.

Studies in diabetic animal models have corroborated the contribution of systemic endotoxemia, microglial activation, and proinflammatory cytokines to DR pathogenesis and retinal tissue damage (Chen et al., 2012; Grigsby et al., 2014; Mendiola et al., 2016; Roy et al., 2017). In the human diabetic retina, while the presence of fibrin(ogen) has been detected, little progress has been made in characterizing links between inflammatory and vascular pathology hallmarks in the context of post-mortem histology, and many questions remain about associations between biomarkers of DR found in patient fluid samples and those detectable in post-mortem tissues (Murata et al., 1992).

In the central nervous system (CNS), microglia constitutively express the CX3CR1 receptor, which binds to its neuronal-derived ligand, fractalkine (FKN). In approximately 20% the human population, the hCX3CR1^{T280M} polymorphic variant gives rise to a CX3CR1 receptor that does not bind strongly to FKN (Cardona et al., 2018). Disrupted FKN-CX3CR1 signaling leads to microglial activation, astrogliosis, IL-1 β production, neuronal loss, and exacerbated neuroinflammation in Ins2^{Akita} and streptozotocin (STZ) murine models of diabetes, with deposits of fibrinogen present at sites of activated perivascular microglia clusters (Cardona et al., 2015; Mendiola et al., 2016). While this phenotype of microgliosis and fibrinogen accumulation is accelerated by acute systemic endotoxemia (Mendiola et al., 2016), the combinatorial effects of microglial dysfunction, systemic inflammation, and vascular damage on visual function have not been investigated. Targeting the coagulation cascade to counteract vascular damage and neuroinflammation has been effective in murine models of Alzheimer's disease (AD) and cerebral malaria (Bergamaschini et al., 2004; Timmer et al., 2010; Wilson et al., 2018). The defibrinogenating agent anacrod has been found to reduce microglial activation and

blood vessel damage in experimental autoimmune encephalomyelitis (EAE), a murine model of multiple sclerosis (MS), but has not been examined in the context of diabetic complications in the CNS (Ryu et al., 2015).

This study aimed to determine the effects of fibrinogen depletion in microglia-mediated inflammation, vascular damage, and vision loss in the diabetic retina. For this, we utilized a two-hit inflammatory diabetic murine model that combines the effects of STZ-mediated hyperglycemia and systemic endotoxemia to more closely mimic the inflammatory microenvironment and vascular pathology observed during DR progression with recurrent acute infections. Results showed that pharmacological fibrinogen reduction in the diabetic retina alleviated microgliosis, fibrinogen deposition and axonal damage, lowered levels of retinal inflammatory mediators, and partially improved vision in diabetic mice. In comparison to human post-mortem tissues from nondiabetic patients, retinas from diabetic patients showed signs of an inflammatory microenvironment, with increased gliosis and associated vascular aberrations. Together, our findings indicate that neuroinflammation and vascular damage in the diabetic retina can be alleviated through systemic defibrinogenation in a CX3CR1-independent manner, which holds therapeutic potential to ameliorate vision deficits in diabetic patients.

Materials and Methods

Post-Mortem Human Patient Tissues

Five nondiabetic and six diabetic human eyes were obtained from the National Disease Research Interchange (Table 1). The post-mortem interval (time in hours from death to procurement) for all tissues was 14 h.

Human Retinal Flat Mounts and Immunofluorescent Staining

Post-mortem whole globes were preserved in 10% formalin at room temperature for a maximum of 48 h. The isolated retina was transferred to a cryoprotection solution until further analyses. For immunofluorescent staining, tissues were subjected to antigen retrieval followed by blocking and permeabilization overnight (ON) at 4°C with 1% Triton-X 100 in 10% normal goat serum (NGS; Jackson ImmunoResearch Laboratories, RRID:AB_2336990) and incubation in primary antibodies for 72 h. at 4°C. After thorough washes (7 \times for 5 min. each, with 0.1% Triton-X in 1 \times PBS), tissues were incubated ON at 4°C in species-specific secondary antibodies, washed and incubated with Hoechst stain for 7 min. at room temperature. Tissues were subsequently mounted on slides using FluorSave reagent (Calbiochem).

Human Eye RNA Isolation and Quantitative PCR

Total RNA was isolated from human tissues using TrizolTM reagent (Invitrogen, RRID:SCR_018519), followed by

Table 1. Human Eye Donor Information.

Donor Tissue Type	Diabetes Type and Duration	Demographic Information		Co-Morbidities
		Sex	Age (Years)	
Nondiabetic	--	F	59	Amyotrophic Lateral Sclerosis Dementia
	--	F	69	Alzheimer's Disease
	--	F	82	Hypertension Peripheral Neuropathy
	--	M	63	Frontal Temporal Dementia
	--	M	81	Hyperlipidemia Hypercholesteremia
Diabetic	T2DM 3 Years	F	57	Hypertension Hyperlipidemia Hypercholesterolemia Myocardial Infarction Multiple Sclerosis Hodgkin's Lymphoma
	T2DM 15 Years	F	73	Hypertension Hyperlipidemia Hypothyroidism Stage IV Kidney Disease Age-Related Macular Degeneration
	T2DM 2 Months	M	59	Possible Sepsis
	T2DM 36 Years	M	61	Hypertension Dyslipidemia Chronic Kidney Disease
	Type Unknown >30 Years	M	72	N/A
	T2DM Duration Unknown	M	73	Hypertension Cerebral Vascular Disease Peripheral Vascular Disease Chronic Obstructive Pulmonary Disease Noonan's Syndrome Chronic Anticoagulation

Note. Human eye donor information provided for the tissues used in histopathological and inflammatory profile analyses, including donor tissue type, diabetes type and duration if known, sex and age of the donor, and relevant co-morbidities.

chloroform extraction and isopropanol precipitation, as previously described (Cardona et al., 2006). Total RNA was purified using RNeasy Mini™ Kit (Qiagen). RNA quality was assessed by agarose gel electrophoresis and RNA concentration was quantitated using a Nanodrop prior to cDNA generation. For quantitative PCR (qPCR), the Biomark HD platform was utilized with a 96.96 Dynamic Array Integrated Fluidic Circuit (IFC) for Gene Expression (Fluidigm). All probes were pre-designed TaqMan gene expression assays using the 5' reporter dye FAM and a 3' minor groove binding (MGB) nonfluorescent quencher (NFQ) (ThermoFisher Scientific). The array format included six technical replicates of each patient sample, three technical replicates of each of the 24 selected retinal genes and housekeeping genes, non-template control, and reverse transcription control (Liu et al., 2016). All quantifications of threshold cycle [C_T] values were normalized to that of the

housekeeping gene peptidyl prolyl isomerase A (PPIA) and analyzed to determine the relative level of gene expression. To compare expression levels of each gene of interest relative to nondiabetic controls, the $\Delta\Delta C_T$ value was calculated as previously described (Livak & Schmittgen, 2001), expressed as log₂ fold change relative to the nondiabetic control group, and depicted to show the extent of upregulation or downregulation in relative gene expression.

Animals

C57BL/6J mice (RRID: IMSR_JAX:000664) and *Cx3cr1*^{gfp/gfp} (CX3CR1-KO) mice were obtained from The Jackson Laboratory, and humanized CX3CR1^{T280M} (hCX3CR1^{T280M}) mice (Cardona et al., 2018) were bred at the University of Texas at San Antonio. Male mice were used in all experiments.

Animal studies were consistent with standards required by the Association for Assessment and Accreditation of Laboratory Animal Care (AAALAC), approved by the Institutional Animal Care and Use Committee, and carried out in accordance with National Institutes of Health (NIH) guidelines.

Diabetic Murine Model

To assess the effects of hyperglycemia and inflammation in diabetic mice, a two-hit inflammatory diabetic murine model was utilized. First, hyperglycemia was induced in male mice at 6–8 weeks of age via intraperitoneal (i.p., 60 mg/kg body weight) injections of streptozotocin (STZ, Sigma-Aldrich). Mice were maintained for a total of 10 or 20 weeks of hyperglycemia. Second, to induce systemic endotoxemia mimicking secondary infections observed in diabetic patients without causing sepsis, mice were injected intraperitoneally with lipopolysaccharide (LPS) (i.p., 20 µg/100 µL PBS/mouse/day; 1 mg/kg of body weight; LPS from *E. coli* serotype 055:B5, Sigma-Aldrich) for 4 consecutive days prior to experiment termination (Cardona et al., 2006; Chen et al., 2012; Fink, 2014; Raduolovic et al., 2018). Mice were euthanized 4 h. after the final LPS injection for analysis as described below.

Glycemic Measurements

Blood glucose levels were measured using the Precision Xtra Blood Glucose Meter (Abbott) and the Clarity BG1000 Blood Glucose Meter (Clarity Diagnostics) and their respective blood glucose test strips. Mice with blood glucose levels >250 mg/dL were considered hyperglycemic.

Depletion of Fibrinogen via Ancrod Injections

Mice were injected intraperitoneally (i.p.) with ancrod (3 IU ancrod/mouse/day, NIBSC) every 12 h. for 14 consecutive days. Age-matched diabetic mice were mock-injected with an equal volume of sterile saline to serve as controls.

Visual Acuity Test

Mice were trained to dig for a food reward by housing them individually and providing them with a 30-mL capacity reward cup containing 1–2 g of a food pellet alongside a small chocolate cereal crumb reward (Cocoa Krispies, Kellogg's) buried beneath fine-grain wood chip bedding (Sani-Chip IRR, LabSupply) mixed with cumin to eliminate olfactory cues.

A visual acuity task was conducted as previously described (Normandin et al., 2022) in a rectangular plexiglass apparatus (13 inches × 9 inches) with two plastic medicine cups containing cumin-scented wood chip bedding embedded in opposite sides of the chamber floor (Keinath et al., 2017). The chamber featured one short wall with 4 diffuse black stripes, and the

other with 2 diffuse black stripes. A high-value chocolate cereal crumb reward was always located in the cup next to the wall with 4 stripes. After mice were food deprived to 80–85% of their *ad libitum* weight using the reward to increase motivation for the task, their visual function was assessed.

During the first two trials, the reward was placed on top of the bedding to reveal the reward location and allow its association with the visual cues. During the third trial, the reward was buried superficially beneath the bedding. During the four subsequent testing trials, the reward was hidden at a consistent depth beneath the top of the bedding in the cup. As a measure of visual acuity, the location of the cup in which the animal first dug was recorded for each trial. Data are presented as the percentage of correct first digs in trials 4–7. To prevent animals from using external auditory and visual cues to locate the reward, a white noise generator was used, and the chamber was surrounded by a black curtain and rotated 90° clockwise relative to the previous trial orientation. To simulate conditions of blindness for control animals, an overhead infrared light was used during trials instead of visible light, and a red-light head lamp was utilized while handling animals during inter-trial periods to eliminate exposure to visible light cues.

Plasma Collection

Under 5% isoflurane anesthesia, murine blood was collected in EDTA-coated tubes (SAI Infusion) prior to perfusion by cardiac puncture using a 1-mL tuberculin syringe. Blood was centrifuged at 2,000 × g for 20 min. at 4°C, and plasma was removed and stored at –80°C after addition of 1 × protease inhibitor cocktail (Roche).

Fibrinogen Enzyme-Linked Immunosorbent Assay

Total plasma fibrinogen levels were determined using the mouse fibrinogen ELISA (Innovative Research) following the manufacturer's instructions and a sample dilution of 1:50,000. Each sample was run in duplicate. Results were reported as milligrams (mg) of fibrinogen per milliliter (mL) of plasma.

Antibodies and Reagents

Supplementary Table 1 lists primary and secondary antibodies used in the studies.

Murine Retina Isolation and Immunofluorescent Staining

Mice were perfused with 1 × Hank's Balanced Salt Solution (Lonza, RRID:SCR_018521) and eyes were fixed in 4% PFA for 20 min. at room temperature. The retina and optic

nerve were isolated as previously described (Park et al., 2017) and then fixed in 1% PFA for 1 h., after which they were transferred to a cryoprotection solution until further analyses. For immunofluorescent staining, retinal flat mounts were blocked and permeabilized ON at 4°C with 1% Triton-X 100 in 10% NGS (Jackson ImmunoResearch Laboratories, RRID: AB_2336990). Tissues were incubated in primary antibodies ON at 4°C, followed by thorough washes (7× for 5 min. each, with 0.1% Triton-X in 1× PBS), and then incubated in species-specific secondary antibodies. Tissues were stained with Hoechst and mounted as described above.

Confocal Microscopy

Confocal microscopy was done using a Zeiss LSM 710 microscope and 3-dimensional z-stack composites of confocal images were generated in Imaris software v7.2 (Bitplane, RRID: SCR_007370). Three random images from the central and peripheral retina per subject or mouse were obtained for further analysis. To quantify fibrinogen, vasculature, axons, and astrocyte immunoreactivity, raw confocal images were uploaded to ImageJ (NIH, RRID:SCR_003070), converted to 32-bit grayscale, and then a global automatic threshold was applied to each image. Fibrinogen, microglia, vasculature, axons, and astrocytic process signal per image were measured and expressed as immunoreactivity percent area of the entire image. For microglial and retinal ganglion cell (RGC) quantification, cells were manually counted in 40× images. Microglial and RGC counts were normalized to volume (i.e., 213 μm × 213 μm × z-stack thickness in μm) and expressed as cells per mm³.

Acellular Capillary Quantification

For histological analysis of retinal capillary degeneration, the retinal vasculature was isolated by the trypsin digest method and stained with Periodic acid Schiff-Hematoxylin (PASH). The number of acellular capillaries was quantified and expressed as acellular capillaries per mm² of retinal vascular area (Kowluru et al., 2001).

Microglial Morphology Quantification

ImageJ analysis software was used to determine the transformation index (TI) of microglia (Fujita et al., 1996). Briefly, the perimeter and area of a microglial cell were measured, and the TI was calculated using the equation $[\text{perimeter}^2/4\pi \times \text{area}^2]$. The TI was determined for five microglia per 40× image from the central and peripheral retina of each mouse, for a total of ten retinal microglia quantified per animal. Values were expressed as a range of 1 to 100, with a TI value of 1 representing a circular object. Therefore, TI values closer to 1 are indicative of reactive, amoeboid cells with fewer and/or shorter cellular processes, while higher TI

values are associated with resting, ramified cells with more and/or longer cellular processes.

Mouse Retinal Cytokine and Chemokine Analysis

Cytokine and chemokine levels in mouse soluble retinal protein extracts were quantitated using the Bio-Plex Pro™ Mouse Cytokine 23-Plex Group I Assay kit (Bio-Rad Laboratories) in accordance with the manufacturer's recommendations. Data from the Bio-Plex assay were acquired and analyzed using the Bio-Plex Manager software (Bio-Rad Laboratories, RRID: SCR_014330). All cytokine concentration measurements were normalized to total soluble protein to yield picograms (pg) of cytokine per milligram (mg) of soluble retinal protein and expressed as fold change relative to nondiabetic controls.

Statistical Analysis

All measurements were plotted as mean ± SD with scatter-dot plots to show the number and distribution of samples. Statistical tests were performed in GraphPad Prism v8. For comparisons between two groups, a Student's t-test was used. Significant differences were defined as P < 0.05 unless stated otherwise. For multiple comparisons, a two-way ANOVA with the Tukey's post-hoc test was performed, using treatment type as the first variable and genotype as the second variable. Significant differences were defined as P < 0.05 unless stated otherwise.

Results

Gene Expression Analysis Reveals Evidence of an Inflammatory Microenvironment in the Human eye

First, we asked whether diabetic patients display evidence of an elevated inflammatory microenvironment in the retina compared to nondiabetic patients (Table 1). To characterize the neuroglial and inflammatory gene expression profile in nondiabetic and diabetic patients, we sought to assess retinal neuronal populations, macroglial activation, microgliosis, and inflammatory processes implicated in DR progression.

We performed quantitative PCR (qPCR) analysis on the following retinal genes: i) genes expressed by retinal neuron populations (PROX1, CALB1, CRX, PRKCA), ii) genes expressed by macroglia (VMAC, GFAP, SYN, NES), iii) genes expressed by microglia (CD68, TMEM119, P2RY12, CX3CR1, CD86); and iv) genes associated with inflammation and neurodegeneration (SIRPA, SIGLEC9, IL-1b, TREM2, MRC1, RAGE1, MERTK). Gene expression analysis by qPCR revealed no statistically significant differences between nondiabetic and diabetic patients overall, although diabetic eyes exhibited upregulation of multiple genes, including calbindin 1 (CALB1), PROX1, and protein kinase C-α (PRKCA), synemin (SYN) and nestin (NES), CD68, CD86, RAGE1, and MER proto-oncogene tyrosine kinase (MERTK) (Figure 1A).

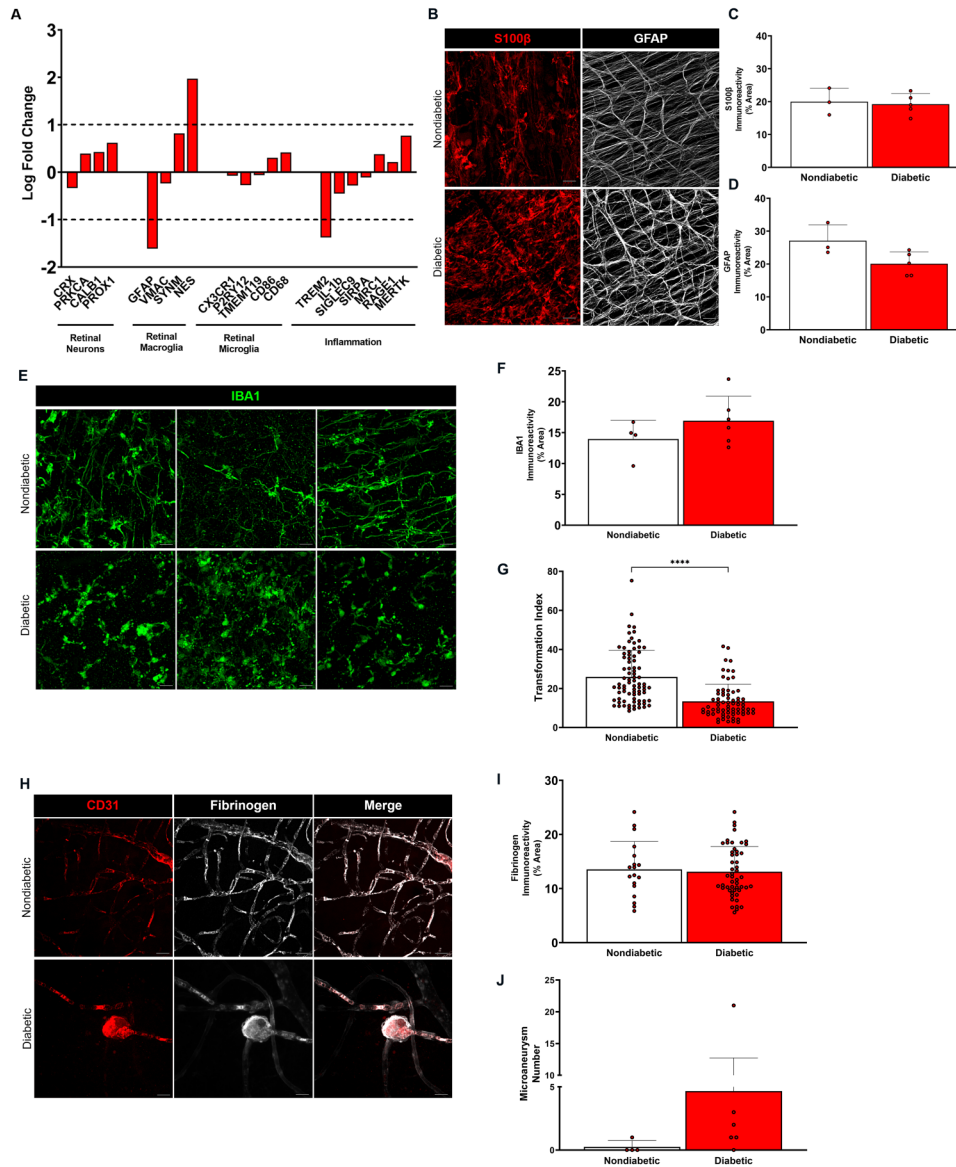


Figure 1. Gene expression and histopathological analyses in the diabetic human eye reveal an inflammatory microenvironment. (A) Relative gene expression levels of neuronal, macroglial, microglial, and inflammatory markers from nondiabetic and diabetic human subject eyes. Peptidyl prolyl isomerase (PPIA) was used as the housekeeping gene and values are expressed as log fold change relative to nondiabetic controls. $n = 3-4$ tissues per group. (B) Confocal images of S100 β ⁺ (red) and GFAP⁺ (white) macroglia in retinal flat mounts from nondiabetic and diabetic human subjects show macroglial processes from astrocytes and Müller cells. (C, D) Quantification of S100 β ⁺ and GFAP⁺ immunoreactivity from central and peripheral regions of retinal flat mounts is shown with each point representing an individual human subject. $n = 3-5$ tissues per group. (E) Confocal images of IBA1⁺ microglia in retinal flat mounts from nondiabetic and diabetic human subjects indicate the presence of higher microglial densities and activation in the diabetic retina compared to the nondiabetic retina. (F, G) Quantification of IBA1⁺ microglia immunoreactivity is shown with each point representing an individual human subject, while morphometric analysis for individual microglial cells is represented as transformation index values. $n = 4$ tissues per group. **** $P < 0.0001$. (H) Confocal images of CD31⁺ retinal vasculature (red) and fibrinogen (white) in retinal flat mounts from nondiabetic and diabetic human subjects show intravascular fibrinogen in the nondiabetic retina and microaneurysms in the diabetic retina. (I, J) Quantification of fibrinogen immunoreactivity and microaneurysms from central and peripheral regions of nondiabetic and diabetic human retinal flat mounts indicates the presence of increased fibrinogen and microvascular abnormalities in the diabetic human retina. $n = 3-4$ tissues per group. Scale bars: 25 μ m.

Microglial Activation and Gliosis are Observed in the Human Retina

To assess inflammation in the human retina, processes of astrocytes and Müller cells using S100 β and glial fibrillary

acidic protein (GFAP) were visualized in flat mounts, and microglia were identified using ionized calcium-binding protein-1 (IBA1). Comparable S100 β ⁺ and GFAP⁺ immunoreactivity was observed in both the nondiabetic and diabetic retina, implying that macroglia elicit similar responses in

the retina (Figure 1B–D). Nondiabetic retinas exhibited ramified microglial cells, indicative of their resting state, while diabetic retinas contained more amoeboid, activated microglia (Figure 1E–F). Statistically significant differences between microglial transformation index (TI) values provided morphometric evidence of higher microglial activation in the diabetic retina (Figure 1G). Together, these results suggest that under conditions of chronic hyperglycemia, microgliosis is characteristic of an elevated inflammatory state in the human eye.

Vascular Aberrations and Fibrinogen Deposition are Evident in the Human Retina

To visualize whether fibrinogen accumulation is observed with vascular alterations in diabetic patients, the endothelial cell marker CD31 was used to identify retinal vasculature, and fibrinogen localization relative to vessels was examined. Fibrinogen was detected within retinal vessels of nondiabetic and diabetic patients (Figure 1H–I). However, in contrast to the nondiabetic retina which lacked vascular outpouchings, all diabetic tissues except one displayed microaneurysms (Figure 1J). Interestingly, fibrinogen also colocalized strongly with microaneurysms along capillaries in the diabetic retina. Overall, these results reveal that fibrinogen accumulation is associated with vascular aberrations and microgliosis in diabetic patients, which supports the rationale of investigating fibrinogen depletion to reduce microglial activation in the diabetic retina.

Chronic Hyperglycemia and CX3CR1 Deficiency may Influence Acellular Capillary Formation

To assess the effects of CX3CR1-mediated inflammation on development of acellular capillaries at a timepoint when little to no hyperglycemia-induced capillary degeneration would be observed, retinal tissues from naïve, nondiabetic LPS-treated, and 20-week diabetic CX3CR1-WT, CX3CR1-KO, and hCX3CR1^{T280M} mice were subjected to trypsin digest, and the number of acellular capillaries was counted. In comparison to naïve and nondiabetic LPS-treated animals from all three genotypes, only some 20-week diabetic CX3CR1-KO animals appeared to have increased acellular capillaries, and the hCX3CR1^{T280M} animals seemed to have an intermediate pathological phenotype (Supplementary Figure 1). Based on these results, chronic hyperglycemia and CX3CR1 deficiency might contribute to the gradual development of vascular pathology in the diabetic retina.

Defibrinogenation Using Ancrod Reduces Plasma Fibrinogen in a Diabetic Murine Model

To investigate the therapeutic potential of selective fibrinogen depletion, the defibrinogenating agent ancrod was administered for 2 weeks to CX3CR1-WT and CX3CR1-KO mice at 8 weeks of diabetes. Age-matched nondiabetic mice with systemic endotoxemia were also assessed to examine effects of

systemic inflammation on circulating fibrinogen levels (Figure 2A). To verify the pathological phenotype, glucose levels in whole blood were measured. Both CX3CR1-WT and CX3CR1-KO animals treated with STZ exhibited hyperglycemia, characterized by significantly higher blood glucose levels compared to naïve and nondiabetic animals (Figure 2B). To determine endogenous plasma fibrinogen levels in healthy mice, plasma was obtained from naïve CX3CR1-WT and CX3CR1-KO mice and compared to fibrinogen-deficient (Fg-KO) mice. While Fg-KO mice expressed no detectable fibrinogen levels in circulation, plasma from naïve CX3CR1-WT and CX3CR1-KO mice contained 1–3 mg/mL fibrinogen (1.82 ± 0.36 and 1.55 ± 0.88 mg/mL, respectively) (Figure 2C). No statistically significant difference was observed in plasma fibrinogen levels when comparing naïve CX3CR1-WT and CX3CR1-KO mice.

Compared to naïve mice, LPS-treated nondiabetic animals from both genotypes displayed lower blood glucose and higher fibrinogen levels (2.36 ± 0.73 and 2.16 ± 0.52 mg/mL, respectively). Plasma of LPS-treated diabetic CX3CR1-WT and CX3CR1-KO mice also contained elevated fibrinogen (2.16 ± 0.55 and 1.71 ± 0.41 mg/mL, respectively) compared to naïve animals (Figure 2C). Next, we asked whether systemic ancrod administration reduces plasma fibrinogen levels. When compared to diabetic animals, ancrod-treated CX3CR1-WT and CX3CR1-KO mice exhibited little to no detectable fibrinogen in plasma (0.022 ± 0.049 and 0.165 ± 0.293 mg/mL, respectively, 2-way ANOVA, $P < 0.0001$), similar to Fg-KO animals. Taken together, these results validate the use of ancrod as an effective pharmacological agent to selectively reduce fibrinogen levels systemically in murine models of inflammatory and vascular diseases.

Defibrinogenation Alters Microglial Morphology and Reduces Microglial Activation

To investigate the effects of fibrinogen depletion on microglial activation, morphometric analysis of retinal microglia was performed by quantifying the transformation index (TI) of IBA1⁺ cells. Overall microglia density was increased in diabetic LPS groups and comparable between naïve and ancrod-treated mice (Figure 3A and B). Diabetic LPS-treated mice exhibited significantly more amoeboid, reactive microglia with lower TI values (18.90 ± 10.7 and 17.53 ± 9.78 , respectively) compared to higher TI values in naïve CX3CR1-WT and CX3CR1-KO retinal microglia (45.71 ± 12.37 and 41.62 ± 17.77 , respectively, 2-way ANOVA, $P < 0.0001$) (Figure 3C). Notably, when compared to diabetic LPS-treated mice, microglia from both ancrod-treated CX3CR1-WT and CX3CR1-KO diabetic mice had higher TI values (31.29 ± 12.33 and 37.37 ± 18.18 , respectively, 2-way ANOVA, $P < 0.0001$) and highly branched morphologies, indicative of a surveillant phenotype. These results show that under conditions of systemic hyperglycemia and inflammation, regardless of

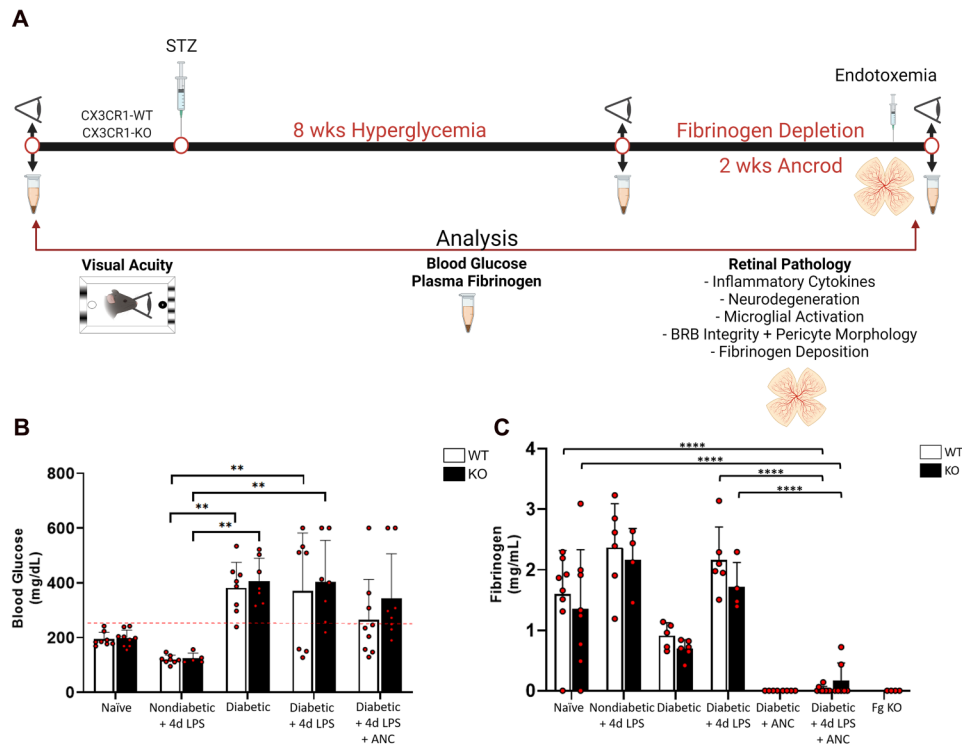


Figure 2. Assessment of pharmacological fibrinogen reduction on hyperglycemia, systemic inflammation, and vision loss in the two-hit diabetic mouse model. (A) Experimental design: Prior to induction of diabetes, a baseline readout of visual acuity and plasma was obtained and whole blood was collected at noted time points to assess fibrinogen levels. To pharmacologically deplete fibrinogen, mice received intraperitoneal injections of anicrod for 2 weeks. Control animals received an equal volume of sterile saline. Visual acuity was assessed prior to LPS and on day 2–4 of the 4d LPS challenge. Animals were euthanized 4 h. after the final anicrod and LPS injections on Day 15 of the anicrod injections to terminate the experiment, and plasma and glycemic measurements were obtained. For retinal pathology analyses, eyes were preserved for immunohistochemical staining of retinal flat mounts. Confocal microscopy was utilized to visualize and quantify microglial activation, neuronal loss, pericyte morphology, vascular damage, and fibrinogen deposition. (B) Glycemic measurements from naïve, nondiabetic, and 10-week diabetic mice under conditions of systemic inflammation, fibrinogen depletion, or both, verify that elevated blood glucose levels are a feature of diabetic animals, which appear to be reduced or masked upon administration of LPS. $n = 5–9$ mice per group. Each point represents data from an individual mouse. (C) Plasma fibrinogen ELISA was performed across the experimental groups. $n = 4–8$ mice per group. Each point represents data from an individual mouse. ** $P < 0.01$, *** $P < 0.001$, **** $P < 0.0001$.

CX3CR1 genotype, anicrod administration decreased morphological changes associated with microglial activation.

Systemic Ancrod Administration Reduces Retinal Fibrinogen Accumulation

To examine the effect of anicrod on fibrinogen accumulation in nondiabetic and diabetic mice exhibiting systemic inflammation, retinal tissue fibrinogen was quantified (Figure 4A). Compared to naïve CX3CR1-WT and CX3CR1-KO mice ($0.153 \pm 0.110\%$ and $0.143 \pm 0.059\%$, respectively), nondiabetic and diabetic LPS-treated CX3CR1-WT and CX3CR1-KO mice displayed increased retinal fibrinogen deposition ($0.628 \pm 0.239\%$ and $0.636 \pm 0.252\%$ in nondiabetic LPS-treated mice, 2-way ANOVA, $P < 0.0001$ and $P = 0.0002$ respectively; and $0.617 \pm 0.178\%$ and $0.367 \pm 0.163\%$ in diabetic LPS-treated mice, 2-way ANOVA, P

< 0.0001 for CX3CR1-WT mice). Importantly, upon anicrod treatment, diabetic CX3CR1-WT and CX3CR1-KO mice had significantly less fibrinogen associated with retinal blood vessels ($0.139 \pm 0.042\%$ and $0.142 \pm 0.038\%$, respectively, 2-way ANOVA, $P < 0.0001$), comparable to fibrinogen observed in naïve retinas (Figure 4B). These results indicate that systemic defibrinogenation ameliorated fibrinogen deposition during DR.

Defibrinogenation Improves Visual Acuity in Diabetic Mice

To assess visual acuity, a two-choice discrimination task was utilized (Figure 5A and B) as previously described (Normandin et al., 2022). To establish an initial baseline readout of visual acuity, naïve CX3CR1-WT and CX3CR1-KO mice were assessed under infrared and visible light conditions. Because mice have significantly impaired

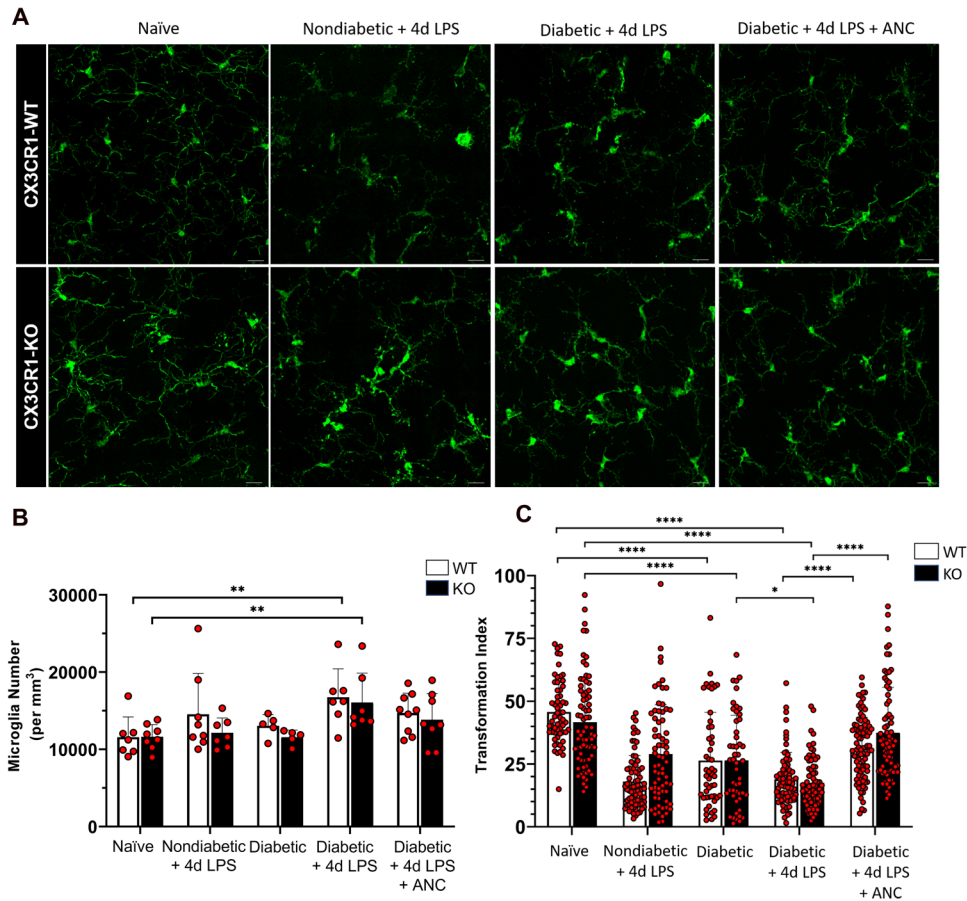


Figure 3. Fibrinogen depletion reduces microglial activation in the diabetic murine retina. (A) Confocal images of IBA1⁺ microglia from 10-week nondiabetic and diabetic LPS-treated CX3CR1-WT and CX3CR1-KO mice show activated microglia with less ramification in comparison to highly ramified microglia with small soma in the naïve retina. Depletion of fibrinogen with ancred shifts activated microglia towards increased ramification, similar to naïve microglia. (B) Quantification of microglial cell numbers indicates increased proliferation in the diabetic LPS-treated retina relative to the naïve CX3CR1-WT and CX3CR1-KO retina. Each point represents data from an individual mouse. (C) Morphometric analysis of IBA1⁺ microglia in the retinas of CX3CR1-WT and CX3CR1-KO mice by transformation index (TI) calculation reveals ramified microglia with higher TI values in the naïve and ancred-treated diabetic retinas, and increasingly activated microglia with lower TI values in the nondiabetic and diabetic LPS-treated retinas, respectively. Each point represents the TI per individual cell. $n = 5-9$ mice per group. * $P < 0.05$, ** $P < 0.01$, *** $P < 0.001$, **** $P < 0.0001$. Scale bars: 25 μm .

vision in the infrared range, this condition was used as a control to simulate and validate visual impairment. Under infrared light, both CX3CR1-WT and CX3CR1-KO animals performed 50% or less correct digs ($40.63 \pm 12.94\%$ and $41.67 \pm 25\%$, respectively), indicating that when unable to see, they located the reward and completed the task due to random chance. However, under visible light conditions, the same groups of CX3CR1-WT and CX3CR1-KO animals performed the task successfully ($77.78 \pm 8.33\%$ and $83.33 \pm 12.91\%$, respectively, 2-way ANOVA, $P < 0.005$), with more correct digs, indicating higher visual acuity (Figure 5C).

With baseline visual acuity established in naïve animals, we then assessed visual acuity in 10-week diabetic CX3CR1-WT and CX3CR1-KO mice that received either 4d LPS treatment or 14d ancred treatment in addition to 4d LPS treatment. Age-matched 10-week nondiabetic mice

from the respective genotypes were subjected to 4d LPS treatment to investigate the effects of acute inflammation alone on visual function. Compared to naïve animals, in visible light, 10-week diabetic CX3CR1-WT and CX3CR1-KO animals with systemic inflammation showed worse visual acuity ($21.43 \pm 9.45\%$ and $28.57 \pm 22.45\%$, respectively, 2-way ANOVA, $P < 0.0001$), performing the task successfully during less than 30% of the trials (Figure 5C). These results indicate that the combinatory effects of inflammation and hyperglycemia in these mice correlated with reduced visual function. In contrast, 10-week diabetic CX3CR1-WT and CX3CR1-KO animals treated with ancred performed better than the diabetic controls that received LPS ($42.59 \pm 16.9\%$ and $56.25 \pm 25.88\%$, respectively), indicating that ancred appears promising in alleviating visual acuity in more than 60% of the wild-type mice.

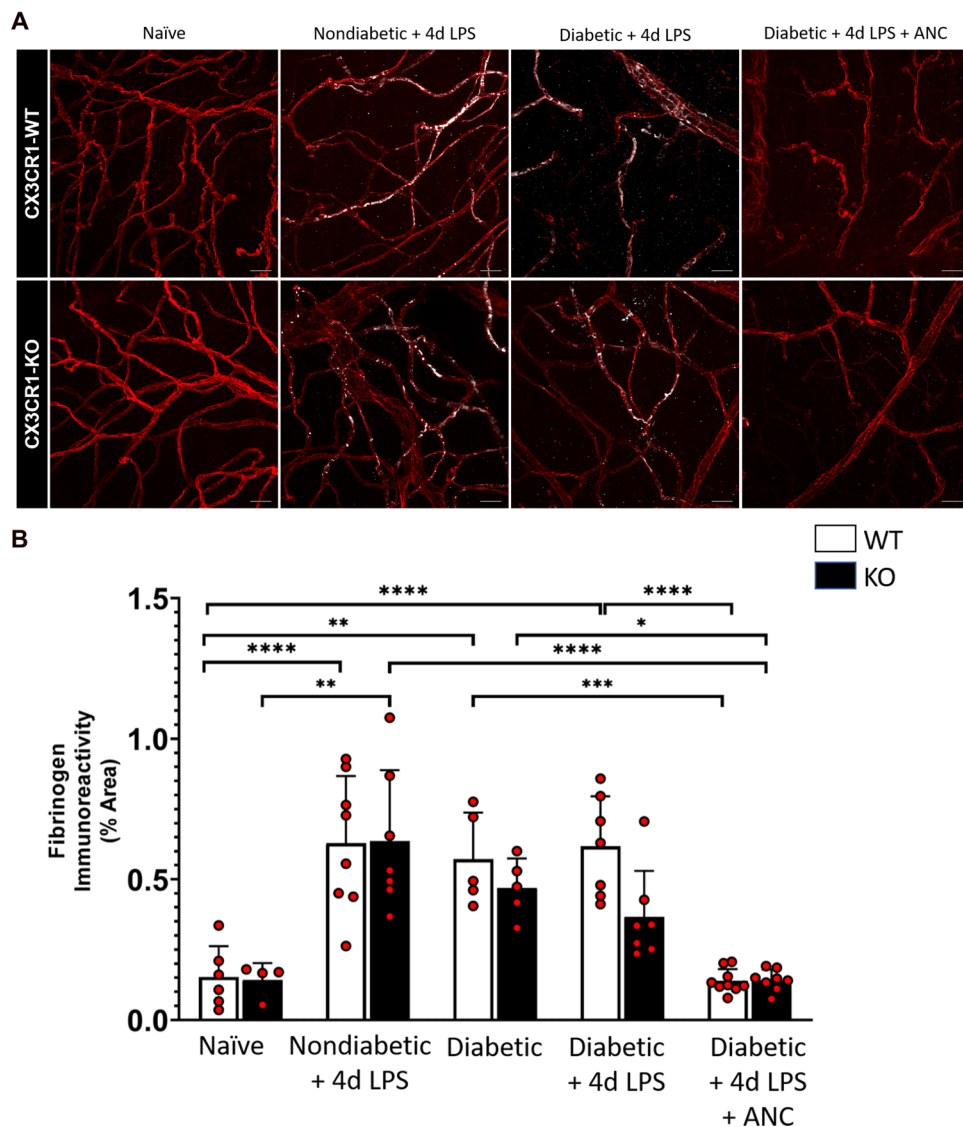


Figure 4. Systemic anacrod administration reduces retinal fibrinogen accumulation in the diabetic murine retina. (A) Confocal images of retinas from 10-week nondiabetic and diabetic LPS-treated CX3CR1-WT and CX3CR1-KO mice display fibrinogen deposits (white) along CD31⁺ retinal vessels (red), which are not detectable in the anacrod-treated diabetic retina. (B) Quantification of fibrinogen in retinal tissues indicates elevated fibrinogen accumulation in retinas of nondiabetic and diabetic LPS-treated mice relative to naïve and anacrod-treated diabetic mice. $n=4-9$ mice per group. Each point represents data from an individual mouse. * $P < 0.05$, ** $P < 0.01$, *** $P < 0.001$, **** $P < 0.0001$. Scale bars: 25 μm .

Systemic Fibrinogen Depletion Preserves Retinal Ganglion Cell Axons in the Diabetic Retina

To investigate the impact of fibrinogen depletion on retinal ganglion cells, the number of NeuN⁺ neurons and the TUJ1⁺ axon immunoreactivity in the RGC layer were assessed across central and peripheral regions of the retina. While no statistically significant differences in RGC soma number were observed in LPS-treated and diabetic CX3CR1-WT and CX3CR1-KO mice (Supplementary Figure 2), hyperglycemia and endotoxemia appeared to affect axons (Figure 6). In comparison to naïve CX3CR1-WT and CX3CR1-KO mice ($31.299 \pm 3.772\%$ and $29.847 \pm 1.395\%$, respectively), 10-week diabetic

CX3CR1-WT and CX3CR1-KO mice exhibited significantly lower TUJ1⁺ immunoreactive area in the retina ($19.627 \pm 1.320\%$ and $20.577 \pm 3.391\%$, 2-way ANOVA, $P < 0.0001$ and $P = 0.001$, respectively). Similarly, when compared to naïve mice, LPS-treated 10-week diabetic CX3CR1-WT and CX3CR1-KO mice showed a significant reduction in TUJ1 immunoreactivity ($19.431 \pm 1.675\%$ and $19.968 \pm 4.396\%$, 2-way ANOVA, $P < 0.0001$ and $P = 0.0004$, respectively). Notably, LPS-treated 10-week diabetic CX3CR1-WT and CX3CR1-KO mice showed an increase in TUJ1⁺ area in response to anacrod ($30.806 \pm 3.733\%$ and $28.613 \pm 3.972\%$, 2-way ANOVA, $P < 0.0001$ and $P = 0.0025$, respectively).

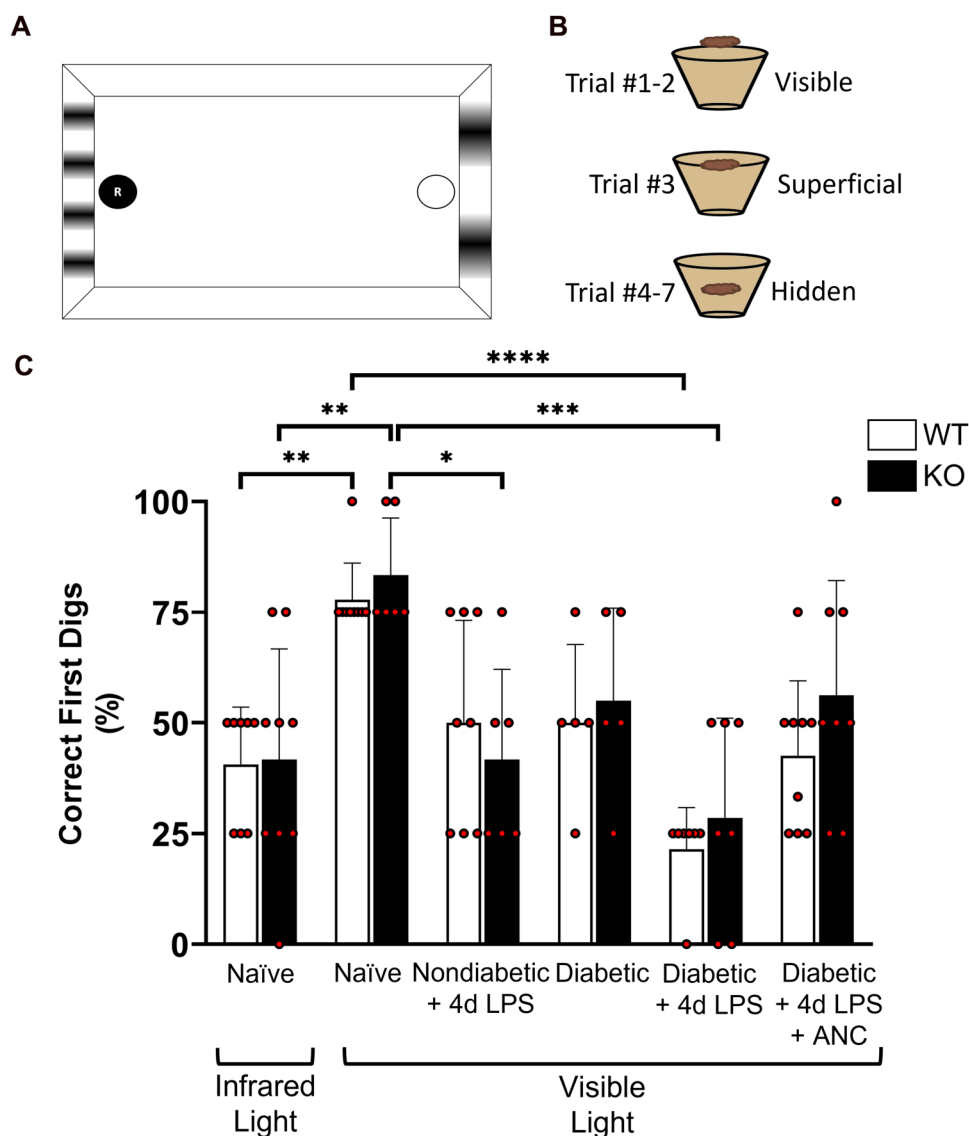


Figure 5. Defibrinogenation improves visual acuity in diabetic mice. (A, B) Schematic layout of the visual acuity cues and location of the high-value food reward during each trial in the two-choice discrimination task chamber. (C) Quantification of the percentage of correct first dig location per animal indicates that 10-week diabetic LPS-treated mice in visible light conditions perform in a manner comparable to sighted naïve animals placed in infrared light (non-sighted) conditions. Treatment to reduce fibrinogen systemically using anicrod improves visual acuity in 10-week diabetic animals compared to untreated diabetic animals. $n = 5-9$ mice per group. Each point represents data from an individual mouse. * $P < 0.05$, ** $P < 0.01$, **** $P < 0.0001$.

Overall, these results suggest that, irrespective of CX3CR1 genotype, hyperglycemia and endotoxemia contribute to axonopathy and that depletion of fibrinogen rescues axons in the diabetic retina during early DR.

Fibrinogen Depletion Dampens Inflammatory Cytokine and Chemokine Expression in the Diabetic Retina

To determine if fibrinogen depletion alters retinal inflammation in mice during early diabetes, inflammatory

cytokine and chemokine profile analysis was conducted in retinal protein extracts. Overall, no differences between diabetic CX3CR1-WT and CX3CR1-KO mice compared to nondiabetic control mice were observed (Table 2).

Cytokines with a 3-fold or greater increase in the diabetic CX3CR1-WT retina included IL-3 and IL-12 (p70), while those in the diabetic CX3CR1-KO retina included IL-9, IFN- γ , IL-13, IL-1 β , IL-17A, TNF- α , IL-6, IL-4, IL-5, IL-10, IL-3, and IL-12 (p70). Upregulated chemokines that increased by more than 3-fold in the diabetic CX3CR1-WT

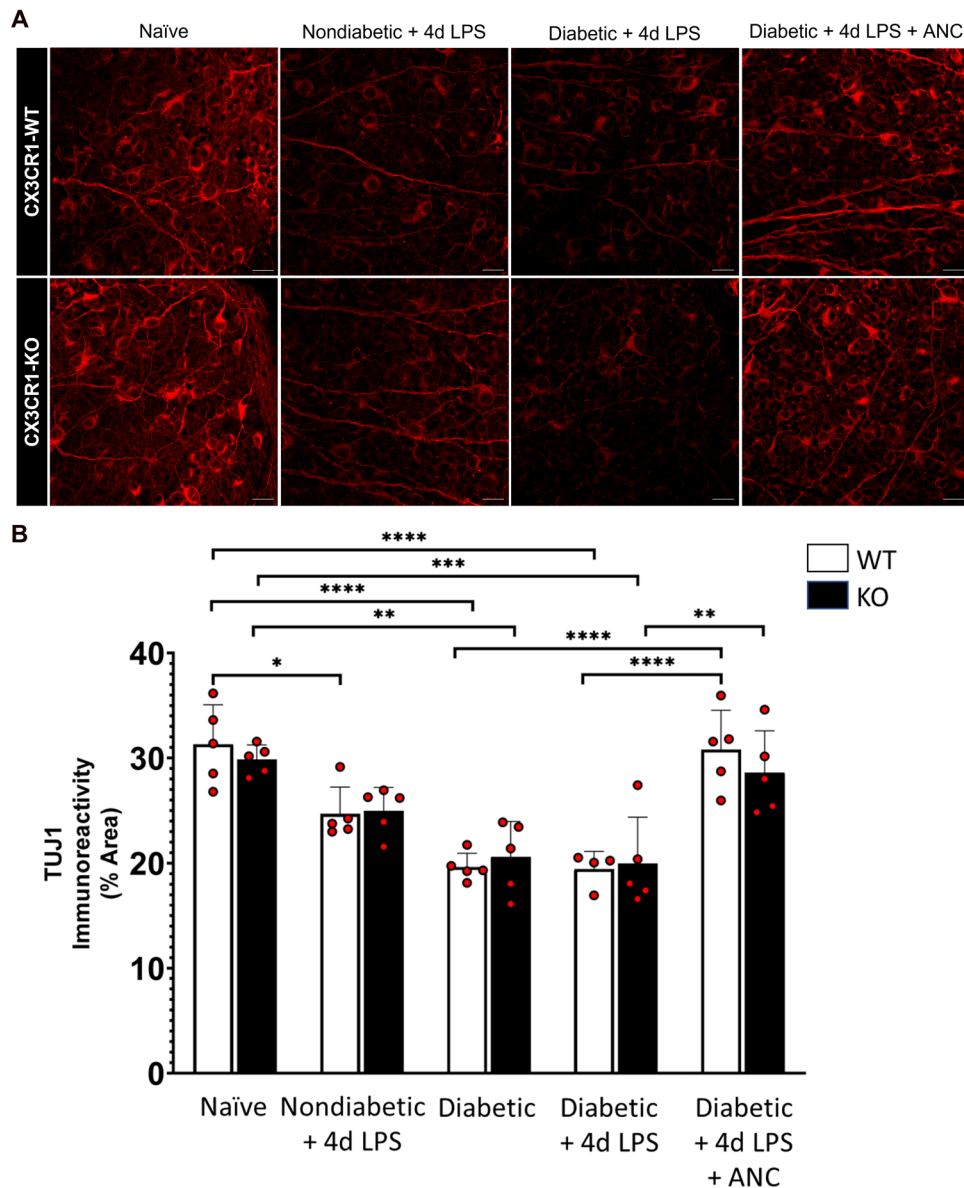


Figure 6. Systemic fibrinogen depletion preserves axons in the diabetic retina. (A) Confocal images of retinas from 10-week nondiabetic and diabetic LPS-treated CX3CR1-WT and CX3CR1-KO mice show TUJ1⁺ axons (red) which are less dense in comparison to axons in the retinas of naïve and ancred-treated diabetic mice. (B) Quantification of TUJ1 immunoreactivity in retinal tissues reveals decreased TUJ1⁺ area in the retinas of nondiabetic and diabetic LPS-treated CX3CR1-WT and CX3CR1-KO mice relative to naïve mice. Ancred-treated diabetic CX3CR1-WT and CX3CR1-KO mice exhibit increased TUJ1⁺ axonal area compared to diabetic LPS-treated mice. $n = 5-9$ mice per group. Each point represents data from an individual mouse. * $P < 0.05$, ** $P < 0.01$, *** $P < 0.001$, **** $P < 0.0001$. Scale bars: 25 μm .

retina were GM-CSF, eotaxin, MIP-1 β , and G-CSF. Chemokines that increased at least 3.5-fold in the CX3CR1-KO retina included GM-CSF, MIP-1 β , KC, and G-CSF. Upon ancred administration, the expression of these cytokines and chemokines was significantly reduced, irrespective of genotype (Figure 7). Taken together, our findings indicate that the inflammatory pathology observed in the diabetic retina can be alleviated through the selective pharmacological depletion of fibrinogen in diabetes.

Discussion

Previously published studies using 10-week diabetic Ins2^{Akita} mice revealed that systemic endotoxemia induced by LPS challenge was associated with accelerated blood-retinal barrier damage in the retina, as indicated by increased retinal fibrinogen deposition and microglial immunoreactivity in Akita-KO mice compared to Akita-HET mice (Mendiola et al., 2016). However, due to the absence of wild-type mice for comparison in these earlier studies, and because

Table 2. Inflammatory Mediator Profile in the Mouse Retina.

Mediator	Diabetic		Ancrod	
	WT	KO	WT	KO
IL-1 α	2.922	2.114	0.856	0.515
IL-1 β	3.179	3.418	0.379	0.306
IL-2	2.788	2.400	1.055	0.714
IL-3	3.565	4.564	0.042	0.008
IL-4	2.883	4.046	0.175	0.149
IL-5	3.026	4.259	0.118	0.118
IL-6	2.930	3.816	0.272	0.202
IL-9	2.748	3.003	0.449	0.357
IL-10	3.308	4.367	0.029	0.079
IL-12 (p40)	3.208	4.253	0.268	0.117
IL-12 (p70)	3.503	5.341	0.085	0.132
IL-13	2.919	3.244	0.374	0.346
IL-17A	3.119	3.423	0.101	0.068
Eotaxin	3.209	3.444	0.393	0.347
G-CSF	3.370	4.842	2.249	0.532
GM-CSF	3.004	3.543	0.087	0.020
IFN- γ	2.861	3.111	0.473	0.384
KC	2.797	3.621	0.572	0.295
MCP-1	2.875	3.245	0.379	0.191
MIP-1 α	3.025	4.192	3.154	1.120
MIP-1 β	3.259	3.604	0.113	0.054
RANTES	2.656	2.184	0.901	0.586
TNF- α	3.394	3.799	0.262	0.389

Note. Inflammatory mediator levels in the diabetic and ancrod-treated diabetic mouse retina denoted as fold change values relative to naïve CX3CR1-WT and CX3CR1-KO mice, respectively. All cytokine and chemokine concentrations (obtained in pg per mL) were normalized to the amount of soluble protein per retinal extract sample, yielding the amount of inflammatory mediator within the murine retina in pg of mediator per mg of retinal protein. The respective fold change values, shown in the table, were calculated using the mean normalized inflammatory mediator values from naïve retinas for each genotype. n = 5–8 mice per group.

Ins2^{Akita} mice become hyperglycemic by 4–5 weeks of age, this prompted further investigation into the effects of hyperglycemia and systemic inflammation on microglia-mediated retinal damage. To that end, in this study, we used a two-hit inflammatory diabetic murine model to mimic the elevated systemic inflammatory status that has been characterized in human diabetic patient studies (Vujosevic & Simo, 2017). Our data shows that depletion of fibrinogen resulted in decreased microglial morphological activation, preserved axonal integrity, and decreased inflammation.

To determine whether selectively targeting fibrinogen could alleviate detrimental neuroglial dysregulation, inflammation, and vascular aberrations in acute DR, we pharmacologically depleted fibrinogen using ancrod in 10-week diabetic CX3CR1-WT and CX3CR1-KO mice and assessed the effects on retinal pathology and visual function. While no statistically significant differences were observed in neuronal soma and pericyte numbers (Supplementary Figures 2 and 3), we found that ancrod treatment altered microglial morphology (Figure 3), reduced fibrinogen accumulation

(Figure 4), and rescued axons in the diabetic retina, irrespective of the CX3CR1 genotype (Figure 6).

Widely used retinal function assays, such as electroretinography and the optokinetic reflex test, are useful in providing information about electrical potentials of retinal neuron populations, and optokinetic nystagmus and optomotor tracking in animals, respectively (Aung et al., 2013; Thyagarajan et al., 2010). However, these responses to visual stimuli do not provide readouts correlating to cortical function and integrated visual performance (Busse et al., 2011; Storchi et al., 2019). To address limitations of reflex-based visual function tests, we applied a two-choice visual acuity test (Keinath et al., 2017; Normandin et al., 2022). Our results show that both systemic endotoxemia and 10-week hyperglycemia resulted in significantly compromised visual function. Although no significant differences between genotypes were noted, 66% of the diabetic ancrod-treated CX3CR1-WT mice performed better than their corresponding non-ancrod controls (Figure 5). These findings further confirm that systemic inflammation impacts retinal integrity, and it is plausible that repeated incidents of inflammation accelerate axonal damage in the diabetic retina. Future studies to increase the assay's sensitivity, such as a modified pentagon-shaped arena, would be relevant to yield a baseline under infrared conditions below 25%. This would potentially facilitate a more accurate assessment of the functional effects of ancrod.

The anti-inflammatory effects of ancrod in our diabetic retinopathy model suggest that the inflammatory environment in the retina facilitates microgliosis and axonal damage. Similar to our observations, ancrod treatment in MS murine models reduced microglial activation, rescued demyelination, increased motor strength, and improved coordination (Adams et al., 2007). In addition, *Cx3cr1^{GFP/+}Fib^{390-396A}* mice, which lack the binding motif required for fibrinogen to interact with microglia via the CD11b/CD18 receptor, showed significantly less microgliosis and neurodegeneration (Davalos et al., 2012). It is possible that eliminating the microglial CD11b/CD18 integrin receptor fibrinogen-binding motif in our diabetic murine model will lend additional clarity regarding the mechanism by which fibrin(ogen) acts as a proinflammatory trigger for retinal microglial activation and axonopathy in DR.

While inflammatory mediators have been assessed in serum, aqueous, and vitreous from diabetic patients and animals, the effects of fibrinogen depletion on the inflammatory profile in diabetes have not yet been examined. Diabetic patients (with and without DR) exhibit increased vitreous levels of IL-1 α and IFN- γ (Bromberg-White et al., 2013; Burgos et al., 1997; Jain et al., 2013; Vujosevic et al., 2016; Wu et al., 2017), and DR patients have significantly higher levels of IL-1 β , IL-2, IL-4, IL-5, IL-6, IL-10, IL-13, GM-CSF, MCP-1 (Adamiec-Mroczek et al., 2009; Bromberg-White et al., 2013; Kim et al., 2015; Mao & Yan, 2014; Schoenberger et al., 2012; Wu et al., 2017), RANTES (Meleth et al., 2005; Vujosevic et al., 2016), and TNF- α (Adamiec-Mroczek

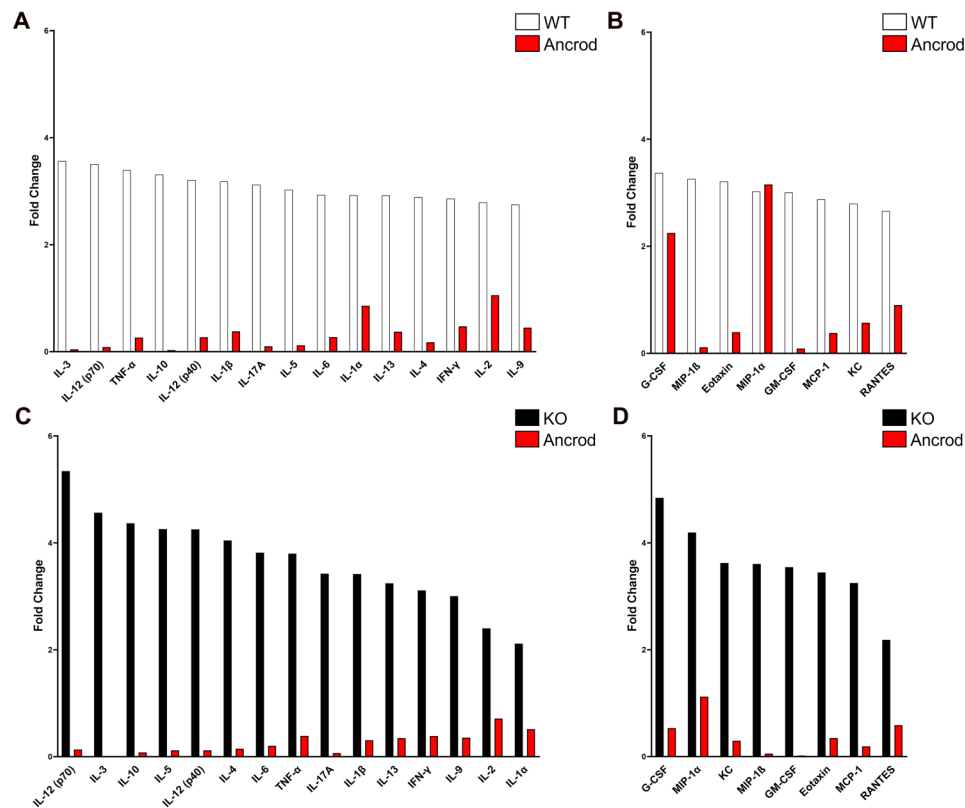


Figure 7. Systemic fibrinogen depletion reduces retinal inflammatory mediators in the diabetic murine retina. (A, B) Inflammatory profile analysis of retinal protein extracts from 10-week diabetic CX3CR1-WT mice (white) reveals elevated cytokine and chemokine levels relative to naïve controls. In the ancrod-treated diabetic retina (red), expression of most inflammatory mediators is comparable to naïve conditions. $n = 5-8$ mice per group. (C, D) Inflammatory profile analysis of retinal protein extracts from 10-week diabetic CX3CR1-KO mice (black) shows elevated cytokine and chemokine levels relative to naïve controls. In the ancrod-treated diabetic retina (red), expression of inflammatory mediators is reduced to levels comparable to or lower than naïve conditions. $n = 5-8$ mice per group.

et al., 2009; Boss et al., 2017; Doganay et al., 2002; Schoenberger et al., 2012; Wu et al., 2017). Similarly, our murine inflammatory profile analyses revealed significantly increased expression of the cytokines IL-12 and IL-3, in addition to the chemokine G-CSF in the retinas of 10-week diabetic mice, which were reduced to levels comparable to naïve mice after ancrod treatment (Table 2; Figure 7). Since these inflammatory mediators are secreted by microglia, macroglia, and activated RGCs under conditions of hyperglycemia and oxidative stress (Vujosevic et al., 2016), it is likely that as DR progresses, neuroglial dysfunction is propagated and exacerbated by the persistent presence of proinflammatory cytokines while anti-inflammatory cytokines attempt to counteract the surrounding tissue damage. IL-12 is involved in angiogenesis and reduced pathological neovascularization in murine models of oxygen-induced retinopathy and chronic ischemia during diabetes (Ali et al., 2017; Zhou et al., 2016). Although the role of IL-3 in DR pathogenesis is unclear, a study revealed that upon mechanical strain to rat RGCs, P2X7 receptors on the neuronal membrane were autostimulated and that neuronal survival was associated with IL-3 and IL-3Ra expression in the RGC layer (Lim

et al., 2016). Based on our findings, it is plausible that hyperglycemia and retinal inflammation contribute to neuronal stress, triggering cytokine release from not only glial cells but also RGCs, which is alleviated by eliminating fibrinogen.

In this study, as previously noted by other groups, we observed large variation in circulating glucose levels in diabetic LPS-treated mouse groups (Figure 2). While some, but not all, mice from each genotype exhibited glucose levels below the hyperglycemia cutoff point of 250 mg/dL, overall, the means for these groups were not statistically different. This variation may be explained by the effects of LPS challenge, which can cause hypoglycemia (Raetzsch et al., 2009). It is known that acute endotoxemia increases glucose-stimulated insulin secretion and glucose clearance, which is regulated by glucagon-like peptide 1 (Nguyen et al., 2014). Although these findings suggest that acute endotoxemia may increase insulin secretion, resulting in lower circulating blood glucose, the impact of recurrent infections and elevated serum LPS levels in diabetic patients warrants further investigation.

In human nondiabetic and diabetic retinas, we looked specifically at associations between vascular abnormalities,

fibrinogen, and glial cells in retinal flat mounts, which facilitated a thorough, 3-dimensional visualization of vasculature and associated glial cells throughout the entire retinal tissue (Figure 1). We detected greater microglial activation in diabetic retinas, along with fibrinogen deposits localized to vascular outpouchings. The proinflammatory cytokines and oxidative stress responses associated with aging and neurodegenerative diseases among the nondiabetic patient cohort in this study could explain the variability in our results, especially regarding the macroglial markers S100 β and GFAP, which are elevated in human serum during stress responses (Malan et al., 2020). Accessing and analyzing human retinal tissues is a challenge, firstly due to the limited tissue banks that allow for effective processing of available post-mortem donor tissues, and secondly because of the associated comorbidities among the control donor tissue group. Histological analyses of the small cohort in this study did not reveal statistically significant differences with regards to glial densities or vascular damage. However, significant microglial activation was revealed through morphometric analysis and positive trends were noted in microgliosis and fibrinogen immunoreactivity within the diabetic group, highlighting the value of assessing retinal flat mount tissues for signs of inflammation, neuroglial dysfunction, and vascular alterations in human diabetic eyes alongside well-established animal models of DR.

Harnessing the potential of targeting fibrinogen in neuroinflammatory and vascular diseases is an important step towards creating more selective, novel modalities to improve sight and cognition. As an alternative to depleting fibrinogen with purified anicrod, there may be therapeutic value in inhibiting interactions between microglia and fibrinogen using small molecules that interfere with the adhesion process mediated by the integrin CD11b/CD18 receptor. Known CD11b/CD18 antagonists include the CD11b/CD18, IB4, and 44a monoclonal antibodies (Park et al., 2007; Wright et al., 1988). A high-throughput screening of more than 100,000 small molecules yielded several novel compounds that block adhesion of C57BL/6 wild-type mouse neutrophils to fibrinogen (Faridi et al., 2010). Additionally, long-term treatment with the small molecule RU-505 significantly reduced microglial activation and fibrinogen deposition in the cortex of AD mice (Ahn et al., 2014). Based on our findings, it is of great interest to investigate the possibility of a therapeutic regimen that combines the anti-inflammatory effects of fractalkine with the neuroprotective and vasoprotective aspects of anicrod. This will enable the development of carefully controlled anti-inflammatory treatments that may be applied to target inflammation and neurodegeneration in the eye and beyond.

List of Abbreviations

AD Alzheimer's Disease
ANOVA analysis of variance

CNS central nervous system
CRX cone-rod homeobox
DR diabetic retinopathy
EAE experimental autoimmune encephalomyelitis
EDTA ethylenediaminetetraacetic acid
ELISA enzyme-linked immunosorbent assay
FAM fluorescein
FKN fractalkine
GFAP glial fibrillary acidic protein
G-CSF granulocyte colony-stimulating factor
GM-CSF granulocyte-macrophage colony-stimulating factor
HET heterozygous
IBA1 ionized calcium-binding protein
IFC integrated fluidic circuit
IFN interferon
KC keratinocyte-derived cytokine
LPS lipopolysaccharide
LSM laser scanning microscope
MERTK MER proto-oncogene tyrosine kinase
MGB minor groove binding
MIP macrophage inflammatory protein
MS multiple sclerosis
NFQ nonfluorescent quencher
PCR polymerase chain reaction
PFA paraformaldehyde
PPIA peptidyl prolyl isomerase A
RANTES regulated upon activation, normal T cell expressed and presumably secreted
RGC retinal ganglion cell
TNF tumor necrosis factor
STZ streptozotocin
VMAC vimentin-type intermediate filament associated coiled-coil protein

Acknowledgements

The authors would like to acknowledge and thank Dr. Jie Tang for generously performing trypsin digests and quantifying the retinal murine acellular capillaries and Dr. Marc Normandin for kindly providing guidance with execution and interpretation of the visual acuity paradigm included in this study. The authors additionally acknowledge the Cell Analysis Core Facility at the University of Texas at San Antonio for support during this work.

Author Contribution(s)

A.E.C. developed the concept of the study. A.E.C., B.S., and I.A.M. participated in the experimental design. Acquisition of data was conducted by B.S., S.M.C., D.V., K.A.C., C.R., D.R., P.V., and A.S.M. Analysis and interpretation of data were performed by A.E.C., B.S., I.A.M., D.V., T.S.K., P.V., and C.R. The manuscript was drafted by A.E.C. and B.S. All authors approve the version of the document to be published.


Declaration of Conflicting Interests

The author(s) declared no potential conflicts of interest with respect to the research, authorship, and/or publication of this article.

Funding

The author(s) disclosed receipt of the following financial support for the research, authorship, and/or publication of this article: This work was supported by the National Institutes of Health (NIH), University of Texas at San Antonio, (grant number R01EY029913 to A.E.C., R01NS106597 to R.S., R01MH123260-01 to I. A. M., GM060655 to . A. C.) and National Science Foundation (NSF) (grant number NSF1565410 to I. A. M.).

ORCID iD

Astrid E. Cardona  <https://orcid.org/0000-0002-5093-8078>

Supplemental Material

Supplemental material for this article is available online.

References

- Adamic-Mroczek, J., Oficjalska-Mlynczak, J., & Misiuk-Hojlo, M. (2009). Proliferative diabetic retinopathy—the influence of diabetes control on the activation of the intraocular molecule system. *Diabetes Research and Clinical Practice*, *84*(1), 46–50. <https://doi.org/10.1016/j.diabres.2009.01.012>
- Adams, R. A., Bauer, J., Flick, M. J., Sikorski, S. L., Nuriel, T., Lassmann, H., Degen, J. L., & Akassoglou, K. (2007). The fibrin-derived $\gamma^{377-395}$ peptide inhibits microglia activation and suppresses relapsing paralysis in central nervous system autoimmune disease. *Journal of Experimental Medicine*, *204*(3), 571–582. <https://doi.org/10.1084/jem.20061931>
- Ahn, H. J., Glickman, J. F., Poon, K. L., Zamolodchikov, D., Jno-Charles, O. C., Norris, E. H., & Strickland, S. (2014). A novel Abeta-fibrinogen interaction inhibitor rescues altered thrombosis and cognitive decline in Alzheimer's disease mice. *Journal of Experimental Medicine*, *211*(6), 1049–1062. <https://doi.org/10.1084/jem.20131751>
- Ali, M., Mali, V., Haddox, S., AbdelGhany, S. M., El-Deek, S. E. M., Abulfadl, A., Matrougui, K., & Belmadani, S. (2017). Essential role of IL-12 in angiogenesis in type 2 diabetes. *American Journal of Pathology*, *187*(11), 2590–2601. <https://doi.org/10.1016/j.ajpath.2017.07.021>
- Aung, M. H., Kim, M. K., Olson, D. E., Thule, P. M., & Pardue, M. T. (2013). Early visual deficits in streptozotocin-induced diabetic long evans rats. *Investigative Ophthalmology & Visual Science*, *54*(2), 1370–1377. <https://doi.org/10.1167/iovs.12-10927>
- Bergamaschini, L., Rossi, E., Storini, C., Pizzimenti, S., Distaso, M., Perego, C., De Luigi, A., Vergani, C., & De Simoni, M. G. (2004). Peripheral treatment with enoxaparin, a low molecular weight heparin, reduces plaques and beta-amyloid accumulation in a mouse model of Alzheimer's disease. *Journal of Neuroscience*, *24*(17), 4181–4186. <https://doi.org/10.1523/JNEUROSCI.0550-04.2004>
- Boss, J. D., Singh, P. K., Pandya, H. K., Tosi, J., Kim, C., Tewari, A., Juzych, M. S., Abrams, G. W., & Kumar, A. (2017). Assessment of neurotrophins and inflammatory mediators in vitreous of patients with diabetic retinopathy. *Investigative Ophthalmology & Visual Science*, *58*(12), 5594–5603. <https://doi.org/10.1167/iovs.17-21973>
- Bromberg-White, J. L., Glazer, L., Downer, R., Furge, K., Boguslawski, E., & Duesbery, N. S. (2013). Identification of VEGF-independent cytokines in proliferative diabetic retinopathy vitreous. *Investigative Ophthalmology & Visual Science*, *54*(10), 6472–6480. <https://doi.org/10.1167/iovs.13-12518>
- Burgos, R., Simo, R., Audi, L., Mateo, C., Mesa, J., Garcia-Ramirez, M., & Carrascosa, A. (1997). Vitreous levels of vascular endothelial growth factor are not influenced by its serum concentrations in diabetic retinopathy. *Diabetologia*, *40*(9), 1107–1109. <https://doi.org/10.1007/s001250050794>
- Busse, L., Ayaz, A., Dhruv, N. T., Katzner, S., Saleem, A. B., Scholvinck, M. L., Zaharia, A. D., & Carandini, M. (2011). The detection of visual contrast in the behaving mouse. *Journal of Neuroscience*, *31*(31), 11351–11361. <https://doi.org/10.1523/JNEUROSCI.6689-10.2011>
- Cardona, A. E., Pioro, E. P., Sasse, M. E., Kostenko, V., Cardona, S. M., Dijkstra, I. M., Huang, D., Kidd, G., Dombrowski, S., Dutta, R., Lee, J. C., Cook, D. N., Jung, S., Lira, S. A., Littman, D. R., & Ransohoff, R. M. (2006). Control of microglial neurotoxicity by the fractalkine receptor. *Nature Neuroscience*, *9*(7), 917–924. <https://doi.org/10.1038/nn1715>
- Cardona, S. M., Kim, S. V., Church, K. A., Torres, V. O., Cleary, I. A., Mendiola, A. S., Saville, S. P., Watowich, S. S., Parker-Thornburg, J., Soto-Ospina, A., Araque, P., Ransohoff, R. M., & Cardona, A. E. (2018). Role of the fractalkine receptor in CNS autoimmune inflammation: New approach utilizing a mouse model expressing the human CX3CR1(I249/M280) variant. *Frontiers in Cellular Neuroscience*, *12*(October Article 365), 1–17. <https://doi.org/10.3389/fncel.2018.00365>
- Cardona, S. M., Mendiola, A. S., Yang, Y. C., Adkins, S. L., Torres, V., & Cardona, A. E. (2015). Disruption of fractalkine signaling leads to microglial activation and neuronal damage in the diabetic retina. *ASN Neuro*, *7*(5), 1–18. <https://doi.org/10.1177/1759091415608204>
- Chen, Z., Jalabi, W., Shpargel, K. B., Farabaugh, K. T., Dutta, R., Yin, X., Kidd, G. J., Bergmann, C. C., Stohlman, S. A., & Trapp, B. D. (2012). Lipopolysaccharide-induced microglial activation and neuroprotection against experimental brain injury is independent of hematogenous TLR4. *Journal of Neuroscience*, *32*(24), 11706–11715. <https://doi.org/10.1523/JNEUROSCI.0730-12.2012>
- Davalos, D., Ryu, J. K., Merlini, M., Baeten, K. M., Le Moan, N., Petersen, M. A., Deerinck, T. J., Smirnov, D. S., Bedard, C., Hakoziaki, H., Gonias Murray, S., Ling, J. B., Lassmann, H., Degen, J. L., Ellisman, M. H., & Akassoglou, K. (2012). Fibrinogen-induced perivascular microglial clustering is required for the development of axonal damage in neuroinflammation. *Nature Communications*, *3*(1227), 1–15. <https://doi.org/10.1038/ncomms2230>
- Doganay, S., Evereklioglu, C., Er, H., Turkoz, Y., Sevinc, A., Mehmet, N., & Savli, H. (2002). Comparison of serum NO, TNF-alpha, IL-1beta, sIL-2R, IL-6 and IL-8 levels with grades of retinopathy in patients with diabetes mellitus. *Eye (Lond)*, *16*(2), 163–170. <https://doi.org/10.1038/sj.eye.6700095>
- Faridi, M. H., Maignel, D., Brown, B. T., Suyama, E., Barth, C. J., Hedrick, M., Vasile, S., Sergienko, E., Schurer, S., & Gupta, V. (2010). High-throughput screening based identification of small molecule antagonists of integrin CD11b/CD18 ligand binding.

- Biochemical and Biophysical Research Communications*, 394(1), 194–199. <https://doi.org/10.1016/j.bbrc.2010.02.151>
- Festa, A., D'Agostino, R. Jr., Tracy, R. P., Haffner, S. M., & Insulin Resistance Atherosclerosis, S. (2002). Elevated levels of acute-phase proteins and plasminogen activator inhibitor-1 predict the development of type 2 diabetes: The insulin resistance atherosclerosis study. *Diabetes*, 51(4), 1131–1137. <https://doi.org/10.2337/diabetes.51.4.1131>
- Fink, M. P. (2014). Animal models of sepsis. *Virulence*, 5(1), 143–153. <https://doi.org/10.4161/viru.26083>
- Fujita, H., Tanaka, J., Toku, K., Tateishi, N., Suzuki, Y., Matsuda, S., Sakanaka, M., & Maeda, N. (1996). Effects of GM-CSF and ordinary supplements on the ramification of microglia in culture: A morphometrical study. *Glia*, 18(4), 269–281. [https://doi.org/10.1002/\(sici\)1098-1136\(199612\)18:4<269::aid-glia2>3.0.co;2-t](https://doi.org/10.1002/(sici)1098-1136(199612)18:4<269::aid-glia2>3.0.co;2-t)
- Funatsu, H., Yamashita, H., Sakata, K., Noma, H., Mimura, T., Suzuki, M., Eguchi, S., & Hori, S. (2005). Vitreous levels of vascular endothelial growth factor and intercellular adhesion molecule 1 are related to diabetic macular edema. *Ophthalmology*, 112(5), 806–816. <https://doi.org/10.1016/j.opthta.2004.11.045>
- Grigsby, J. G., Cardona, S. M., Pouw, C. E., Muniz, A., Mendiola, A. S., Tsin, A. T., Allen, D. M., & Cardona, A. E. (2014). The role of microglia in diabetic retinopathy. *Journal of Ophthalmology*, 2014(705783), 1–15. <https://doi.org/10.1155/2014/705783>
- Jain, A., Saxena, S., Khanna, V. K., Shukla, R. K., & Meyer, C. H. (2013). Status of serum VEGF and ICAM-1 and its association with external limiting membrane and inner segment-outer segment junction disruption in type 2 diabetes mellitus. *Molecular Vision*, 19, 1760–1768. <http://www.molvis.org/molvis/v19/1760>
- Keinath, A. T., Julian, J. B., Epstein, R. A., & Muzzio, I. A. (2017). Environmental geometry aligns the hippocampal map during spatial reorientation. *Current Biology*, 27(3), 309–317. <https://doi.org/10.1016/j.cub.2016.11.046>
- Kern, T. S. (2007). Contributions of inflammatory processes to the development of the early stages of diabetic retinopathy. *Experimental Diabetes Research*, 2007(95103), 1–14. <https://doi.org/10.1155/2007/95103>
- Kim, M., Kim, Y., & Lee, S. (2015). Comparison of aqueous concentrations of angiogenic and inflammatory cytokines based on optical coherence tomography patterns of diabetic macular edema. *Indian Journal of Ophthalmology*, 63(4), 312–317. <https://doi.org/10.4103/0301-4738.158069>
- Klaassen, I., de Vries, E. W., Vogels, I. M. C., van Kampen, A. H. C., Bosscha, M. I., Steel, D. H. W., Van Noorden, C. J. F., Lesnik-Oberstein, S. Y., & Schlingemann, R. O. (2017). Identification of proteins associated with clinical and pathological features of proliferative diabetic retinopathy in vitreous and fibrovascular membranes. *PLoS One*, 12(11), e0187304, 1–21. <https://doi.org/10.1371/journal.pone.0187304>
- Kowluru, R. A., Tang, J., & Kern, T. S. (2001). Abnormalities of retinal metabolism in diabetes and experimental galactosemia. VII. Effect of long-term administration of antioxidants on the development of retinopathy. *Diabetes*, 50(8), 1938–1942. <https://doi.org/10.2337/diabetes.50.8.1938>
- Lim, J. C., Lu, W., Beckel, J. M., & Mitchell, C. H. (2016). Neuronal release of cytokine IL-3 triggered by mechanosensitive autostimulation of the P2X7 receptor is neuroprotective. *Frontiers in Cellular Neuroscience*, 10(270), 1–11. <https://doi.org/10.3389/fncel.2016.00270>
- Liu, X., Xie, J., Liu, Z., Gong, Q., Tian, R., & Su, G. (2016). Identification and validation of reference genes for quantitative RT-PCR analysis of retinal pigment epithelium cells under hypoxia and/or hyperglycemia. *Gene*, 580(1), 41–46. <https://doi.org/10.1016/j.gene.2016.01.001>
- Livak, K. J., & Schmittgen, T. D. (2001). Analysis of relative gene expression data using real-time quantitative PCR and the 2(-delta delta C(T)) method. *Methods (San Diego, Calif.)*, 25(4), 402–408. <https://doi.org/10.1006/meth.2001.1262>
- Loukovaara, S., Koivunen, P., Ingles, M., Escobar, J., Vento, M., & Andersson, S. (2014). Elevated protein carbonyl and HIF-1alpha levels in eyes with proliferative diabetic retinopathy. *Acta Ophthalmologica*, 92(4), 323–327. <https://doi.org/10.1111/aos.12186>
- Malan, L., Hamer, M., von Känel, R., van Wyk, R. D., Wentzel, A., Steyn, H. S., van Vuuren, P., & Malan, N. T. (2020). Retinal-glia ischemia and inflammation induced by chronic stress: The SABPA study. *Brain, Behavior, & Immunity - Health*, 2(2020), 100027, 1–9. <https://doi.org/10.1016/j.bbih.2019.100027>
- Mao, C., & Yan, H. (2014). Roles of elevated intravitreal IL-1beta and IL-10 levels in proliferative diabetic retinopathy. *Indian Journal of Ophthalmology*, 62(6), 699–701. <https://doi.org/10.4103/0301-4738.136220>
- Meleth, A. D., Agro'n, E., Chan, C-C., Reed, G. F., Arora, K., Byrnes, G., Csaky, K. G., Ferris, F. L., & Chew, E. Y. (2005). Serum inflammatory markers in diabetic retinopathy. *Investigative Ophthalmology & Visual Science*, 46(11), 4295. <https://doi.org/10.1167/iovs.04-1057>
- Mendiola, A. S., Garza, R., Cardona, S. M., Mythen, S. A., Lira, S. A., Akassoglou, K., & Cardona, A. E. (2016). Fractalkine signaling attenuates perivascular clustering of microglia and fibrinogen leakage during systemic inflammation in mouse models of diabetic retinopathy. *Frontiers in Cellular Neuroscience*, 10(303), 1–15. <https://doi.org/10.3389/fncel.2016.00303>
- Murata, T., Ishibashi, T., & Inomata, H. (1992). Immunohistochemical detection of extravasated fibrinogen (fibrin) in human diabetic retina. *Graefes Archive for Clinical and Experimental Ophthalmology*, 230(5), 428–431. <https://doi.org/10.1007/BF00175927>
- Nguyen, A. T., Mandard, S., Dray, C., Deckert, V., Valet, P., Besnard, P., Drucker, D. J., Lagrost, L., & Grober, J. (2014). Lipopolysaccharides-mediated increase in glucose-stimulated insulin secretion: Involvement of the GLP-1 pathway. *Diabetes*, 63(2), 471–482. <https://doi.org/10.2337/db13-0903>
- Normandin, M. E., Garza, M. C., Ramos-Alvarez, M. M., Julian, J. B., Eresanara, T., Punjaala, N., Vasquez, J. H., Lopez, M. R., & Muzzio, I. A. (2022). Navigable space and traversable edges differentially influence reorientation in sighted and blind mice. *Psychological Science*, 33(6), 925–947. <https://doi.org/10.1177/09567976211055373>
- Park, D. Y., Lee, J., Kim, J., Kim, K., Hong, S., Han, S., Kubota, Y., Augustin, H. G., Ding, L., Kim, J. W., Kim, H., He, Y., Adams, R. H., & Koh, G. Y. (2017). Plastic roles of pericytes in the blood-retinal barrier. *Nature Communications*, 8(15296), 1–16. <https://doi.org/10.1038/ncomms15296>
- Park, J. Y., Arnaout, M. A., & Gupta, V. (2007). A simple, no-wash cell adhesion-based high-throughput assay for the discovery of small-molecule regulators of the integrin CD11b/CD18.

- Journal of Biomolecular Screening*, 12(3), 406–417. <https://doi.org/10.1177/1087057106299162>
- Radulovic, K., Mak'Anyengo, R., Kaya, B., Steinert, A., & Niess, J. H. (2018). Injections of lipopolysaccharide into mice to mimic entrance of microbial-derived products after intestinal barrier breach. *Journal of Visualized Experiments: JoVE*, e57610(135), 1–9. <https://doi.org/10.3791/57610>
- Raetzsch, C. F., Brooks, N. L., Alderman, J. M., Moore, K. S., Hosick, P. A., Klebanov, S., Akira, S., Bear, J. E., Baldwin, A. S., Mackman, N., & Combs, T. P. (2009). Lipopolysaccharide inhibition of glucose production through the toll-like receptor-4, myeloid differentiation factor 88, and nuclear factor kappa b pathway. *Hepatology*, 50(2), 592–600. <https://doi.org/10.1002/hep.22999>
- Roy, S., Kern, T. S., Song, B., & Stuebe, C. (2017). Mechanistic insights into pathological changes in the diabetic retina: Implications for targeting diabetic retinopathy. *American Journal of Pathology*, 187(1), 9–19. <https://doi.org/10.1016/j.ajpath.2016.08.022>
- Ryu, J. K., Petersen, M. A., Murray, S. G., Baeten, K. M., Meyer-Franke, A., Chan, J. P., Vagena, E., Bedard, C., Machado, M. R., Rios Coronado, P. E., Prod'homme, T., Charo, I. F., Lassmann, H., Degen, J. L., Zamvil, S. S., & Akassoglou, K. (2015). Blood coagulation protein fibrinogen promotes autoimmunity and demyelination via chemokine release and antigen presentation. *Nature Communications*, 6(8164), 1–15. <https://doi.org/10.1038/ncomms9164>
- Schoenberger, S. D., Kim, S. J., Sheng, J., Rezaei, K. A., Lalezary, M., & Cherney, E. (2012). Increased prostaglandin E2 (PGE2) levels in proliferative diabetic retinopathy, and correlation with VEGF and inflammatory cytokines. *Investigative Ophthalmology & Visual Science*, 53(9), 5906–5911. <https://doi.org/10.1167/iovs.12-10410>
- Spranger, J., Kroke, A., Mohlig, M., Hoffmann, K., Bergmann, M. M., Ristow, M., Boeing, H., & Pfeiffer, A. F. (2003). Inflammatory cytokines and the risk to develop type 2 diabetes: Results of the prospective population-based European prospective investigation into cancer and nutrition (EPIC)-potsdam study. *Diabetes*, 52(3), 812–817. <https://doi.org/10.2337/diabetes.52.3.812>
- Storchi, R., Rodgers, J., Gracey, M., Martial, F. P., Wynne, J., Ryan, S., Twining, C. J., Cootes, T. F., Killick, R., & Lucas, R. J. (2019). Measuring vision using innate behaviours in mice with intact and impaired retina function. *Scientific Reports*, 9(1), 10396, 1–16. <https://doi.org/10.1038/s41598-019-46836-y>
- Thyagarajan, S., van Wyk, M., Lehmann, K., Lowel, S., Feng, G., & Wässle, H. (2010). Visual function in mice with photoreceptor degeneration and transgenic expression of channelrhodopsin 2 in ganglion cells. *Journal of Neuroscience*, 30(26), 8745–8758. <https://doi.org/10.1523/JNEUROSCI.4417-09.2010>
- Timmer, N. M., van Dijk, L., van der Zee, C. E., Kiliaan, A., de Waal, R. M., & Verbeek, M. M. (2010). Enoxaparin treatment administered at both early and late stages of amyloid beta deposition improves cognition of APPswe/PS1dE9 mice with differential effects on brain Aβ levels. *Neurobiology of Disease*, 40(1), 340–347. <https://doi.org/10.1016/j.nbd.2010.06.008>
- Vujosevic, S., Micera, A., Bini, S., Berton, M., Esposito, G., & Midea, E. (2016). Proteome analysis of retinal glia cells-related inflammatory cytokines in the aqueous humour of diabetic patients. *Acta Ophthalmologica*, 94(1), 56–64. <https://doi.org/10.1111/aos.12812>
- Vujosevic, S., & Simo, R. (2017). Local and systemic inflammatory biomarkers of diabetic retinopathy: An integrative approach. *Investigative Ophthalmology & Visual Science*, 58(6), BIO68–BIO75. <https://doi.org/10.1167/iovs.17-21769>
- Wang, X., Wang, G., & Wang, Y. (2009). Intravitreal vascular endothelial growth factor and hypoxia-inducible factor 1α in patients with proliferative diabetic retinopathy. *American Journal of Ophthalmology*, 148(6), 883–889. <https://doi.org/10.1016/j.ajo.2009.07.007>
- Wellen, K. E., & Hotamisligil, G. S. (2005). Inflammation, stress, and diabetes. *Journal of Clinical Investigation*, 115(5), 1111–1119. <https://doi.org/10.1172/JCI25102>
- Wilson, K. D., Ochoa, L. F., Solomon, O. D., Pal, R., Cardona, S. M., Carpio, V. H., Keiser, P. H., Cardona, A. E., Vargas, G., & Stephens, R. (2018). Elimination of intravascular thrombi prevents early mortality and reduces gliosis in hyper-inflammatory experimental cerebral malaria. *Journal of Neuroinflammation*, 15(1), 173. <https://doi.org/10.1186/s12974-018-1207-4>
- Wright, S. D., Weitz, J. I., Huang, A. J., Levin, S. M., Silverstein, S. C., & Loike, J. D. (1988). Complement receptor type three (CD11b/CD18) of human polymorphonuclear leukocytes recognizes fibrinogen. *Proceedings of the National Academy of Sciences of the United States of America*, 85(20), 7734–7738. <https://doi.org/10.1073/pnas.85.20.7734>
- Wu, H., Hwang, D. K., Song, X., & Tao, Y. (2017). Association between aqueous cytokines and diabetic retinopathy stage. *Journal of Ophthalmology*, 2017(9402198), 1–8. <https://doi.org/10.1155/2017/9402198>
- Zhou, Y., Yoshida, S., Kubo, Y., Kobayashi, Y., Nakama, T., Yamaguchi, M., Ishikawa, K., Nakao, S., Ikeda, Y., Ishibashi, T., & Sonoda, K. H. (2016). Interleukin-12 inhibits pathological neovascularization in mouse model of oxygen-induced retinopathy. *Scientific Reports*, 6(28140), 1–9. <https://doi.org/10.1038/srep28140>